Catalysis Today 143 (2009) 326–333

Contents lists available at ScienceDirect

Catalysis Today

journal homepage: www.elsevier.com/locate/cattod

# Identification of the role of surface acidity in the deactivation of $TiO_2$ in the selective photo-oxidation of cyclohexane

María D. Hernández-Alonso *, Ana R. Almeida, Jacob A. Moulijn, Guido Mul

*Catalysis Engineering, Delft University of Technology, Julianalaan 136, 2628 BL Delft, The Netherlands*

ARTICLE INFO

*Article history:*
Available online 14 November 2008

*Keywords:*
Photocatalysis
Selective photo-oxidation
Cyclohexane
Cyclohexanone
$TiO_2$
Anatase
Surface modification
Surface acidity
Zr
ATR
Infrared

ABSTRACT

Anatase-structured $Ti_{1-x}Zr_xO_2$ materials with $x = 0.00$, 0.01 and 0.06, were prepared by a reverse microemulsion method, characterized, and tested as catalysts for the selective photo-oxidation of cyclohexane to cyclohexanone. *In situ* ATR-FTIR spectroscopy was used to evaluate the reaction. Zr incorporation into the anatase lattice enhances the surface acidity of $TiO_2$ without causing any significant structural or electronic modification. As expected, also the stability of surface adsorbed water, i.e. the hydrophilicity, was enhanced. The increase in the Brønsted acidity, together with the higher hydrophilicity, is shown to be detrimental for performance (selectivity and stability) in the selective photo-oxidation of cyclohexane. Apparently potential intrinsic catalytic advantages of having higher acidity are outweighed by (i) the enhanced number of water born $OH^{\bullet}$ radicals, inducing non-selective reactions, and (ii) enhanced hydrophilicity leading to slow desorption and consecutive oxidation of cyclohexanone.

© 2008 Elsevier B.V. All rights reserved.

## 1. Introduction

Cyclohexanone is an important commercial product, used to obtain caprolactam for Nylon-6 production, and currently is obtained by liquid phase selective oxidation of cyclohexane at elevated temperatures and pressures [1]. An alternative to this process is the photocatalytic oxidation of cyclohexane over $TiO_2$ at room temperature and pressure. Research has mainly focussed on the effect of the solvent, photon flux, wavelength and particle size on product formation and selectivity [2–10]. Furthermore, it has been proven that a high oxygen concentration [6], the absence of water in the flow, and a suitable illumination source [8,9] can contribute to enhance the selectivity to cyclohexanone over cyclohexanol in this reaction. The role of the catalyst structure on the activity and selectivity toward ketone formation, have also been studied. The anatase polymorph of $TiO_2$ has shown a higher selectivity to cyclohexanone than rutile [3,4], and particle sizes can be tuned in order to reach an optimum performance [6,7]. Surface characteristics (e.g. surface hydroxyl group density) are also important in determining photocatalytic performance.

Catalyst stability has received relatively little attention in the literature. As has been previously demonstrated, surface carboxylates and carbonates diminish the activity of the photocatalysts [6,9]. The accumulation of these deactivating species, has been proposed to be the result of consecutive oxidation of a cyclohexyl peroxide intermediate or adsorbed cyclohexanone, based on a study applying ATR infrared spectroscopy [10]. Thus, favouring the conversion of the cyclohexyl peroxide to the ketone and/or cyclohexanone desorption in order to limit carboxylate and carbonate accumulation, by modification of the $TiO_2$ surface properties, is the main goal of this research.

Incorporation of $Zr^{4+}$ into the anatase lattice has been proven to produce important changes in the surface characteristics of $TiO_2$, without causing significant structural or electronic modifications (up to ca. 6 at.% Zr content) [11]. Thus, $Ti_{1-x}Zr_xO_2$ photocatalysts with $x = 0.00$, 0.01 and 0.06, prepared by a reverse microemulsion method that yields homogeneous nanocrystals, were characterized and tested in the reaction to evaluate the effect of surface modification on the behaviour of the catalysts in the selective cyclohexane photo-oxidation. *In situ* Attenuated Total Reflectance (ATR)-FTIR spectroscopy was used to follow the reaction. This technique has been used in a wide variety of applications and, recently, has been proven to be a useful tool for studies of liquid phase reactions under working conditions (*operando*) [12]. Both unstable reaction intermediates (peroxides) and species adsorbed on/or interacting with the catalyst surface can be detected. These advantages make this technique very suitable for both kinetic and mechanistic studies of liquid phase selective photo-oxidation,

* Corresponding author. Tel.: +31 152786955; fax: +31 152785006.
*E-mail address:* M.D.HernandezAlonso@tudelft.nl (M.D. Hernández-Alonso).

0920-5861/$ – see front matter © 2008 Elsevier B.V. All rights reserved.
doi:10.1016/j.cattod.2008.09.025

although only few applications of *in situ* ATR-FTIR spectroscopy in heterogeneous photocatalysis have been reported in the literature.

## 2. Experimental procedures

### 2.1. Synthesis procedure and characterization techniques

The samples were prepared by a reverse microemulsion method, similar to that described elsewhere [13]. Ti–Zr solid solutions (hereafter named as TZ*x*, where *x* stands for the Zr content) were obtained by addition of $Ti(OPr^i)_4$ (Aldrich, 97%) dissolved in 2-propanol (Aldrich, 99.5%) to an aqueous solution containing the adequate amount of $ZrO(NO_3)_2{\cdot}6H_2O$ (Aldrich, 99.9%; 50 mL) dispersed in *n*-heptane (Scharlau, 99%; 427 mL) and using Triton X-100 (Aldrich; 89 mL) as surfactant and *n*-hexanol as cosurfactant. The resulting mixture was stirred for 24 h, centrifuged, rinsed with methanol and dried at RT. Finally, the obtained powders were calcined at 773 K for 3 h, applying a ramp rate of 2 K $min^{-1}$. Pure $TiO_2$ was prepared following a similar procedure.

The Zr content of the samples was determined by ICP-AES analysis. The BET surface areas were obtained from $N_2$ adsorption isotherms, measured at 77 K in a Micromeritics 2100 automatic apparatus.

Powder XRD patterns were recorded on a Seifert XRD 3000P diffractometer using Ni-filtered Cu Kα radiation in the Bragg–Brentano geometry. The crystal size was calculated according to the Scherrer equation from the width of the (1 0 1) reflection of anatase, whereas the diffraction line broadening due to the strain was analyzed by the modified Williamson-Hall plots [14].

High resolution transmission electron microscopy (HRTEM) images were recorded in a JEOL 3000F FEG microscope, with a 0.21 nm point resolution. The microscope is equipped with an X-ray Energy Dispersion Spectroscopy (XEDS) microanalysis system (LINK ISIS 300). The micrographs were digitized for image processing and fast Fourier transforms were used to obtain the Digital Diffraction Patterns (DDPs).

The microcalorimetric studies of ammonia adsorption were carried out in a differential heat-flow microcalorimeter of the Tian-calvet type C80 from Setaram, connected to a conventional volumetric apparatus.

DRIFTS studies of samples at elevated temperatures and upon cyclohexane adsorption were carried out with a Thermo Nicolet Nexus spectrometer equipped with a liquid $N_2$-cooled MCT detector and a SpectraTech DRIFT high-temperature cell with $CaF_2$ windows. These spectra were registered after accumulation of 64 scans at a resolution of 4 $cm^{-1}$. A flow of helium at 30 mL $min^{-1}$ was maintained during the measurements. For the adsorption tests, the samples were treated at 393 K for 1 h prior to being exposed to a 30 mL $min^{-1}$ He flow saturated with cyclohexane.

### 2.2. Cyclohexane photo-oxidation experiments

The ATR-FTIR set-up used for these experiments has been described in detail elsewhere [10], and consisted of a Harrick Horizon multiple internal reflections accessory, coupled to a 4 mL flow-through cell containing a ZnSe crystal on the bottom plate and a quartz window on the top plate. The FTIR spectra were registered on a Nicolet 8700 FTIR equipped with a DTGS detector. The reaction mixture was illuminated by means of seven UV LEDs (375 nm wavelength, Roithner Lasertechnik) fitted on the top of the cell. The total estimated light intensity was 3 mW $cm^{-2}$. Oxygen saturated cyclohexane was flown through the ATR cell at 4 mL $min^{-1}$. A suspension of the catalyst in water, previously heated to 393 K for 1 h in static air, using a concentration such to obtain a coating thickness of ca. 1.7 μm, was spread on the ZnSe crystal and dried in vacuum overnight. Prior to the photo-oxidation reaction, adsorption of cyclohexane (99%, J.T. Baker) on the coatings was monitored for 100 min. A mirror velocity of 0.6329 cm $s^{-1}$ and a resolution of 4 $cm^{-1}$ were used for all measurements. Photo-oxidation of cyclohexane was followed for 100 min, taking a spectrum every minute. The temperature in the oxygenation vessel was monitored during experiments by a thermocouple. The outflow of the cell was lead to a chilling bath to maintain the liquid at room temperature.

**Table 1**
Chemical composition and textural data of the photocatalysts.

| Sample | Zr (wt.%) | Formula | $S_{BET}$ ($m^2$ $g^{-1}$) |
|---|---|---|---|
| $TiO_2$ | 0 | $TiO_2$ | 52 |
| TZ1 | 0.96 | $Zr_{0.01}Ti_{0.99}O_2$ | 57 |
| TZ6 | 6.32 | $Zr_{0.06}Ti_{0.94}O_2$ | 71 |

## 3. Results

### 3.1. Structural and surface characterization of the photocatalysts

The composition of the catalysts used in this study is displayed in Table 1, as well as the BET surface area values obtained from the $N_2$ adsorption isotherms at 77 K. It can be observed that the presence of Zr leads to a slight increase in the specific surface area of the obtained $TiO_2$. Structural information obtained from the XRD patterns and HRTEM is presented in Table 2. The anatase phase was the only $TiO_2$ polymorph detected in these materials. The shift of the diffraction peaks to lower diffraction angles is indicative of the formation of solid solutions by addition of $Zr^{4+}$. Because of the larger atomic radius of $Zr^{4+}$, the shift is associated with a larger cell volume. The modification of the structure can be considered insignificant in comparison to the remarkable changes observed previously in $Ti_{1-x}Zr_xO_2$ solid solutions with $x > 0.06$ [11].

The crystallite size of the photocatalysts was calculated by different methods. The Scherrer equation allowed us to estimate the apparent domain size, smaller than the real crystallite size due to the fact that the broadening of the diffraction lines caused by other factors is not taken into account in the calculation. In most of the cases, this additional broadening is due to the presence of distortion effects. The strain can be the result of the presence of oxygen vacancies and different types of defects in the lattice of the nanoparticles. To separate the effect of size and microstrain, the modified Williamson–Hall method, known as Williamson–Hall Integral Breath (WHIB) method was used. The original Williamson–Hall plot [15] considers that broadening functions are Cauchy curves but, particularly for low-strain materials, the strain profile tends to be Gaussian [16]. Williamson–Hall plots can be applied to a Gaussian profile with the integral breath method proposed by Ungár et al. [14,17]. As expected, the crystallite sizes obtained by the WHIB method are bigger than the ones calculated according to the Scherrer equation. A slight increase in the strain values is also

**Table 2**
Structural information from the XRD patterns and HRTEM images.

| Sample | $2\theta$ – (1 0 1) anatase | Unit cell volume (Å$^3$) | Strain, $\xi$[a] | Crystallite size (nm) | | |
|---|---|---|---|---|---|---|
| | | | | Scherrer[b] | WHIB[a] | HRTEM |
| $TiO_2$ | 25.402 | 135.7 | 0.0041 | 12.8 | 14.6 | n.m. |
| TZ1 | 25.356 | 135.9 | 0.0042 | 12.6 | 14.6 | n.m. |
| TZ6 | 25.348 | 135.9 | 0.0044 | 14.3 | 17.0 | 15.1 |

[a] Calculated using the Williamson–Hall Integral Breath method.
[b] Estimated from the most intense peak of the diffraction pattern, using the Scherrer equation; n.m.: not measured.

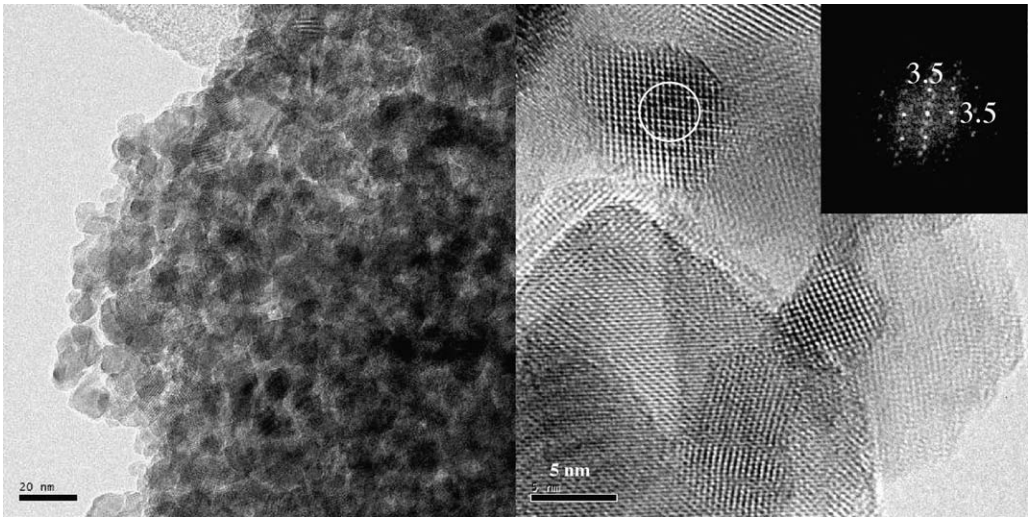


**Fig. 1.** HRTEM images of TZ6. The Digital Diffraction Pattern (DDP) corresponds to the highlighted zone.

observed with Zr content, although it can be considered as not relevant at these doping levels, ruling out any significant structural distortion of the anatase lattice caused by Zr incorporation, as was confirmed by other techniques (e.g. XANES, EXAFS and Raman spectroscopy) [11].

Two HRTEM micrographs of TZ6 are displayed in Fig. 1, along with the DDP of the selected area. This technique confirms the crystallinity of the materials and provides evidence for the absence of extended defects, such as stacking faults or crystal twinning. The DDP shows interplanar spacings (3.5 and 3.5 Å) and angles (81.8°) corresponding to a particle with anatase structure oriented along the [1 1 1] axis. XEDS analysis indicates that the TZ6 catalyst contains on the average 5.2 wt.% Zr. A crystallite size distribution was obtained by measuring the so-called Martin's diameter from different micrographs. The average value, presented in Table 2, is in good agreement with the particle size estimated by the modified Williamson–Hall method, which took into account the contribution of microstrain to the broadening of the diffraction lines, and is just slightly bigger than the value obtained from the Scherrer equation.

Taking into account the results described above and considering also that the band gap does not experience any change in the Ti–Zr samples as compared to pure titania [11], it can be concluded that Zr addition does not lead to structural or electronic modifications of as prepared $TiO_2$. Nevertheless, important changes in the surface characteristics of these materials occur upon Zr incorporation. Although only moderate changes in the specific surface area are observed, properties as surface acidity and hydrophilicity are considerably affected, as will be discussed in the following.

Information about the surface acidity of the various catalysts, extracted from ammonia adsorption microcalorimetry experiments (Fig. 2), is displayed in Table 3. The acid strength of the materials can be compared on the basis of the calculated fraction of

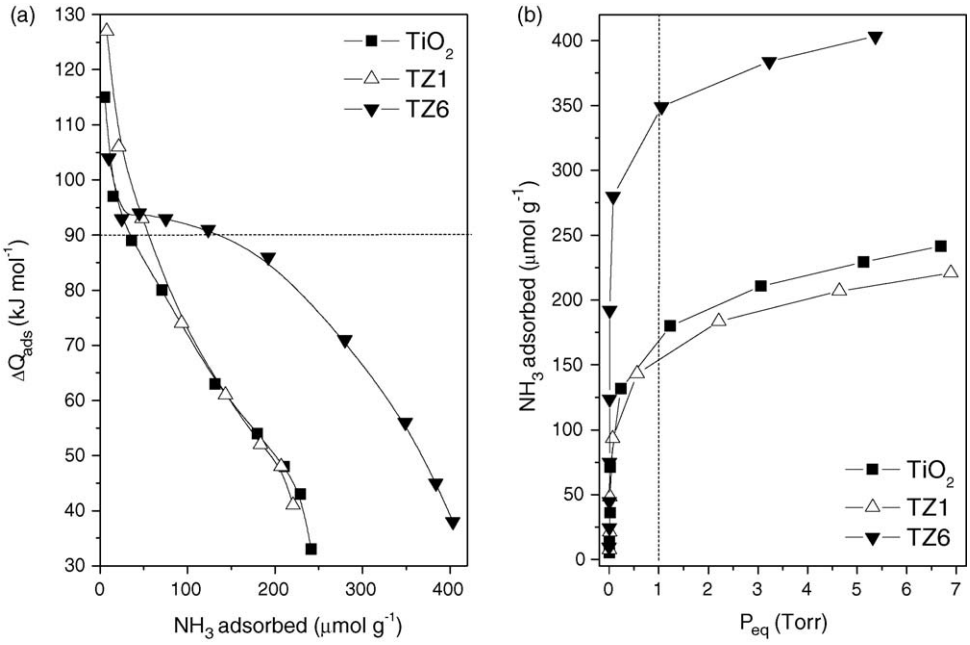


**Fig. 2.** (a) Differential heats for $NH_3$ adsorption, as a function of the adsorbed amount ($\mu$mol $g^{-1}$); (b) adsorption isotherms of $NH_3$.

**Table 3**
Surface acidity as determined by the microcalorimetric studies of ammonia adsorption.

| Sample | $n_T$ (μmol g$^{-1}$) | $n_{90}$ (μmol g$^{-1}$) | $n_{90}/n_T$ ratio |
|---|---|---|---|
| $TiO_2$ | 167.96 | 34.73 | 0.21 |
| TZ1 | 149.98 | 54.64 | 0.36 |
| TZ6 | 344.35 | 135.76 | 0.39 |

sites which gives rise to a differential heat higher than 90 kJ mol$^{-1}$ ($n_{90}$) over the number of total sites ($n_T$), measured at an equilibrium pressure of 1 Torr from the adsorption isotherms. It is clear from the results that surface acidity increases with Zr doping; i.e. a higher number of strong acid sites are present in the solid solutions. In TZ6, both $n_T$ and $n_{90}$ values remarkably rise. A different profile of the calorimetric curve (Fig. 2a) of TZ6 with respect to the undoped $TiO_2$ and TZ1 is apparent. The continuous decrease of the heats of adsorption as long as the coverage increases, indicate a heteregeneous distribution of the acid sites in the first two samples [18,19]. In the case of TZ6, a more homogeneous distribution of sites can be expected. The higher surface acidity in $TiO_2$–$ZrO_2$ systems, that has been previously reported and has been considered as one of the reasons of the increased activity of these materials in photocatalytic reactions [20–22], can be explained using Tanabe's model. This model was proposed to explain the increase in surface acidity observed in binary metallic oxides. For a chemically mixed binary oxide, Tanabe's model [23] considers that the coordination number of the guest cation is maintained in the host oxide lattice and also that the coordination number of all the oxygens in the major component oxide is retained in the binary one (Fig. 3). To keep the electric neutrality, Brønsted acidity (extra protons) is expected to appear when the charge imbalance is negative, while Lewis acid sites will be formed when the charge imbalance is positive. In the case of $TiO_2$–$ZrO_2$ mixed oxides, the increased acidity would be due to a negative charge imbalance created by doping the anatase structure with Zr. The charge imbalance is calculated for each individual bond to the guest cation and multiplied by the number of bonds to that cation. In the $ZrO_2$, each Zr atom is bonded to eight oxygens and each oxygen is bonded to four Zr atoms. In the anatase structure, each Ti is octahedrally coordinated with each oxygen

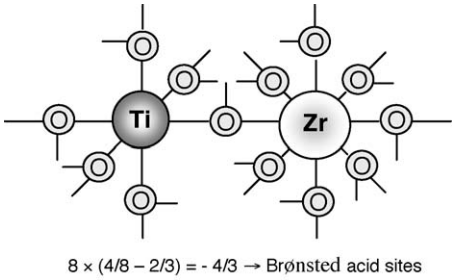


**Fig. 3.** Schematic representation of the Ti–O–Zr bonds, according to the model proposed by Tanabe [23] to explain the increase in surface acidity observed in binary metallic oxides.

bonded to three Ti atoms. Taking this into account, when a Zr atom enters the anatase lattice, each of its eight bonds is now attached to an oxygen bonded only to another two cations. Therefore, four valence electrons on Zr divided by eight bonds, minus two electrons available on the oxygen atom divided by three bonds gives a charge imbalance value of −1/6 per bond (total charge imbalance = −4/3). As a result of this negative imbalance, new Brønsted acid sites will be created from the association of protons with the nearby oxygen atoms [20]. Tanabe's model has proved to have a much higher validity than the previously postulated Thomas' hypothesis [24].

Fig. 4a and b shows detail of the 4000–2500 cm$^{-1}$ region of the DRIFT spectra registered in helium atmosphere, after treating the samples at different temperatures. At RT, the spectrum of $TiO_2$ shows the presence of a broad absorption where two different bands, centered at ca. 3400 and 3120 cm$^{-1}$, are overlapped (Fig. 4a). These bands can be ascribed to the coupled OH stretching modes of H-bonded water from multilayer molecular arrangements. The broad lowest wavenumber feature corresponds to molecules in a relatively ordered arrangement, tetrahedrally bonded to other water molecules by hydrogen bonds [25]. The narrow bands observed at 3695 and 3630 cm$^{-1}$ can be assigned to the stretching modes of Ti–OH in the multilayer water environment. When increasing the temperature to 393 K, water molecules are removed, leading to a decrease in the intensity of the broad bands at 3400 and 3120 cm$^{-1}$. A narrow band at 3670 cm$^{-1}$ arises,

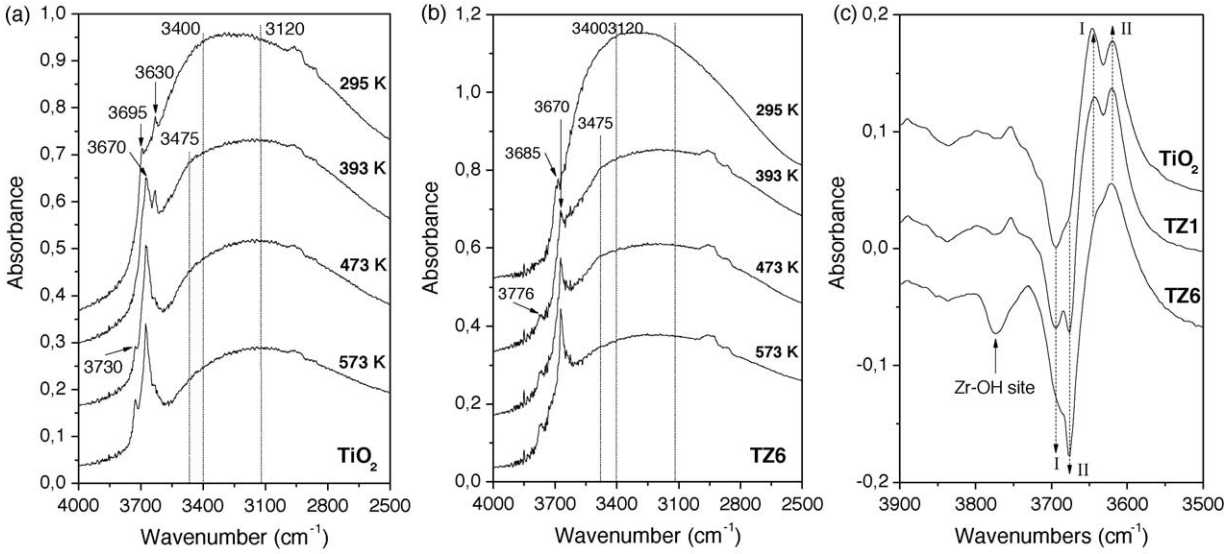


**Fig. 4.** (a) $TiO_2$ and (b) TZ6: detail of the DRIFT spectra of the fresh catalysts, registered in helium atmosphere (30 mL min$^{-1}$), after heating the samples at different temperatures; (c) DRIFT spectra of cyclohexane adsorption on the samples, treated at 393 K prior to adsorption.

that can be ascribed to the stretching mode of bridging hydroxyls, which proton is expected to be weakly bonded [26,27]. At even higher temperatures, an additional band at 3730 $cm^{-1}$ appears that can be assigned to the vibrational mode of terminal OH groups on $Ti^{4+}$ centers. No remarkable differences are observed in the $TiO_2$ and TZ1 (not shown) spectra. In the DRIFT spectra of the TZ6 catalyst (Fig. 4b), a narrow band at 3685 $cm^{-1}$ is observed, related to the stretching mode of free OH from a second water layer [25]. When the sample is heated to 393 K, a new band appears at 3776 $cm^{-1}$ that can be ascribed to the OH stretching mode of terminal Zr–OH groups [28]. The band at 3730 $cm^{-1}$, related to terminal hydroxyls on $Ti^{4+}$ centers, is not clearly detected in the DRIFT spectrum of TZ6. In all the spectra, small bands at 2970, 2940 and 2860 $cm^{-1}$ are also detected, and can be attributed to the presence of residual organic compounds on the catalyst surface.

For the above-described interval (4000–2500 $cm^{-1}$), the area under the curve was calculated and normalized to $S_{BET}$ of the catalysts, to derive a water loss percentage at elevated temperatures. The following decreasing trend was obtained: pure titania (ca. 59%) > TZ1 (51%) > TZ6 (46%). This indicates that water molecules are more strongly bound to the surface of the Zr containing catalysts.

DRIFT spectra of adsorbed cyclohexane, obtained after pretreating the samples at 393 K and using the spectrum of the catalyst prior to being exposed to the gas as background, are shown in Fig. 4c. The negative features at 3695–3670 $cm^{-1}$, together with the absorptions appearing around 3670–3585 $cm^{-1}$, show that cyclohexane may adsorb through H-bridge bonding on, at least, two different types of hydroxyl groups. Considering the relative intensity of these negative and positive features, corresponding to two different peaks (I and II in the figure), it seems that the preferential adsorption sites are different from one sample to another. It is worth noting that in TZ6 catalyst, the terminal hydroxyls on $Zr^{4+}$ centers are also playing an important role in the adsorption of the organic, as reflected by the additional negative band located at 3776 $cm^{-1}$ and the positive absorption associated with it. Minor changes in that spectral range are also observed in $TiO_2$ and TZ1 spectra, which could be tentatively assigned to changes in the surface hydroxyl composition as a result of cyclohexane adsorption. The interaction of liquid phase cyclohexane with the catalyst will be discussed in the following.

### 3.2. Cyclohexane selective photo-oxidation tests

ATR-FTIR spectra of cyclohexane adsorption on the three catalysts, registered once the equilibrium was reached, are displayed in Fig. 5a. Besides the bands corresponding to the vibrations of liquid cyclohexane, whose intensity remains invariable, two bands located at 1162 and 1128 $cm^{-1}$ show a continuous growth with time during cyclohexane adsorption. No remarkable differences are observed between the samples, except for the TZ6 catalyst, where the two characteristic peaks previously mentioned are less clearly resolved. These two peaks correspond to the bands of neat cyclohexane at 1157 and 1090 $cm^{-1}$ that have shifted to higher frequencies upon adsorption on the catalysts surface [29].

In Fig. 5b, the spectra registered after 100 min of irradiation are displayed. Because the ATR-FTIR spectrum recorded at the adsorption equilibrium was used as background for the spectra registered during the photocatalytic oxidation, the bands appearing correspond exclusively to species formed during the reaction. The presence of the negative peaks at 1449, 1257, 1162 and 1128 $cm^{-1}$ is due to the photocatalytic degradation of cyclohexane. The peaks at 1692 and 1713 $cm^{-1}$ correspond to the C=O stretching vibration of adsorbed and desorbed cyclohexanone [10,30], respectively, while the intense peaks at 1592 and 1390 $cm^{-1}$ are assigned to the C=O stretching vibrations of adsorbed carboxylates and carbonates [31]. It is worth noticing that peaks appear at a slightly lower wavenumber in sample TZ6.

Fig. 6a displays the ATR-FTIR spectra registered at different times during the cyclohexane photo-oxidation on $TiO_2$. In the first stage of the reaction, adsorbed cyclohexanone (1692 $cm^{-1}$) is the only product detected on the catalyst surface. After 2 min,

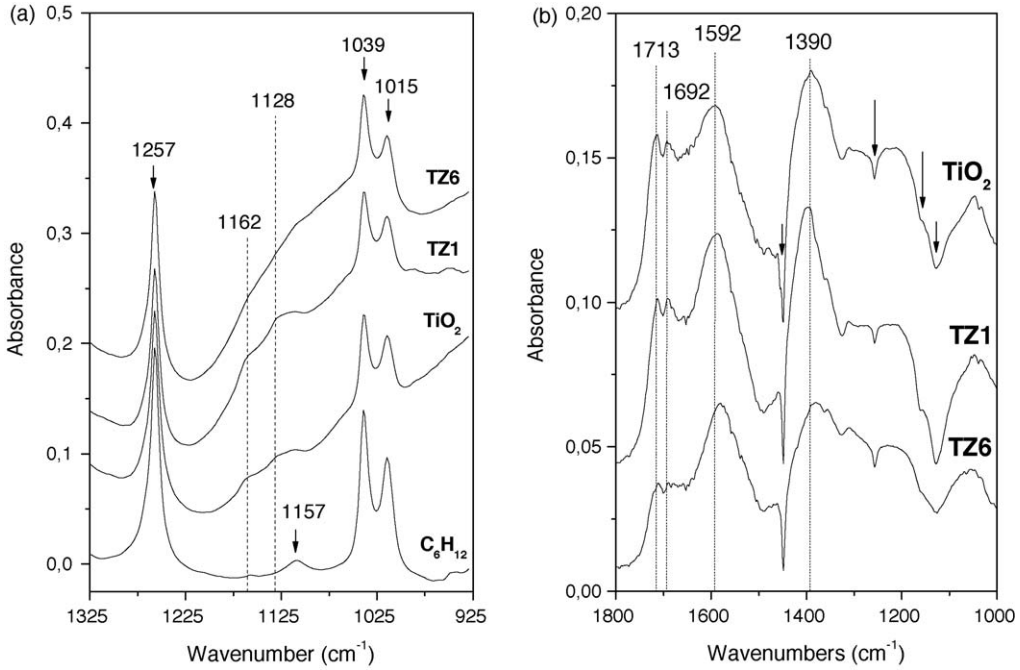


**Fig. 5.** (a) ATR-FTIR spectra of cyclohexane adsorption on the different photocatalysts, coated on a ZnSe crystal and treated at 393 K. The spectrum of each coating on the crystal, in air, was used as the corresponding background; (b) ATR-FTIR spectra of cyclohexane photo-oxidation on the different catalysts tested, recorded after 100 min. Arrows indicate the negative peaks related to the photocatalyzed disappearance of adsorbed cyclohexane.

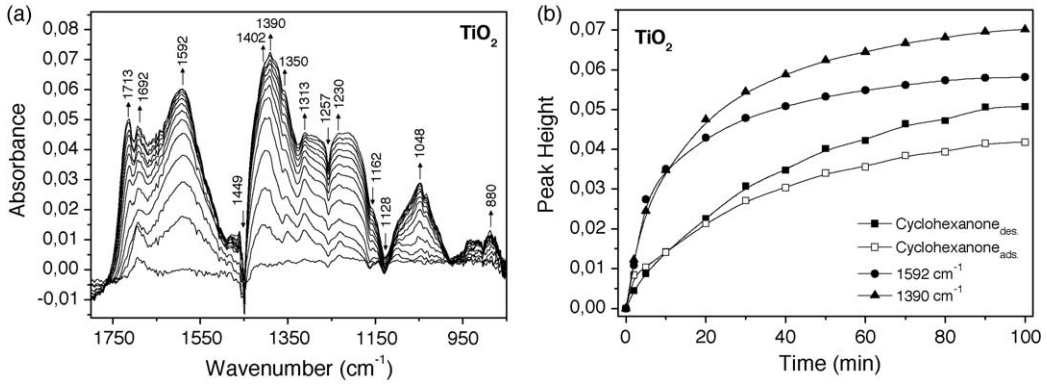


**Fig. 6.** (a) Time-resolved ATR-FTIR spectra of cyclohexane photo-oxidation on $TiO_2$. Spectra recorded at 0.5, 2, 5, 10, 20, 30, 40, 50, 60, 70, 80, 90 and 100 min. Arrows pointing up indicate increasing peaks, and arrows pointing down, decreasing peaks; (b) evolution of the most prominent peaks formed during cyclohexane photo-oxidation on $TiO_2$.

desorption of cyclohexanone into cyclohexane is observed (1713 $cm^{-1}$), and the formation of products by further oxidation is also evident. The unequivocal identification of the different carboxylate and carbonate species that may be simultaneously adsorbed on the catalyst is difficult due to overlapping bands [32,33]. Both carboxylates and carbonates could be contributing to the two intense bands centered at ca. 1592 and 1390 $cm^{-1}$, as well as to the smaller band at ca. 1313 $cm^{-1}$. Peaks at 1230 and 1048 can be assigned to the presence of bidentate and monodentate carbonate compounds [32], while the one at 880 $cm^{-1}$ can be associated with the deformation mode of free carbonate ions [34]. Although cyclohexanol has been reported to be one of the products resulting from the photocatalytic oxidation of cyclohexane [3,5,6], no bands related to the formation of this product were detected under the experimental conditions described in this work.

To analyze the evolution of product formation, the peak height of the different bands was determined. Their relative intensity can provide useful semiquantitative information about the performance of the tested photocatalysts. Peak height evolution of the most prominent features arising during cyclohexane photo-oxidation on $TiO_2$ is shown in Fig. 6b. It is worth noticing that the peaks centered at 1592 and 1390 $cm^{-1}$ follow a different trend after the first 10 min of reaction, pointing out that the main contribution to their intensity is not the same.

For each catalyst, evolution of adsorbed cyclohexane was determined from the analysis of the peak area of bands located at ca. 1162 and 1128 $cm^{-1}$. In this case, peak areas can be calculated due to the absence of overlapping bands in that interval. A commercial photocatalyst, $TiO_2$ Hombikat UV100, was also assayed for comparative reasons. In order to fairly compare the performance of the different photocatalysts, peak area values were normalized by considering the specific surface area of each catalyst and the mass of material employed in the experiment. As shown in Fig. 7a, Hombikat exhibits the highest decomposition rate for cyclohexane, followed by TZ1 and undoped $TiO_2$. The lowest rate was obtained for TZ6.

Fig. 7b shows the progress of cyclohexanone formation over the different photocatalysts. The amount of cyclohexanone formed per unit surface area is higher for the laboratory-prepared $TiO_2$ and decreased considerably with the incorporation of Zr into the anatase lattice. The tested samples show a continuously decreasing cyclohexanone production rate that indicates deactivation of the active sites. The lowest formation rate of cyclohexanone is observed when TZ6 is used as photocatalyst. It is worth noticing that, in spite of the higher activity of TZ1 with respect to $TiO_2$, less cyclohexanone is produced on the Ti–Zr catalyst. Also Hombikat, with the fastest cyclohexane oxidation rate, displays lower cyclohexanone production than titania prepared by the micro-emulsion method.

Since products of further oxidation, carboxylates and carbonates, are formed from the adsorbed cyclohexanone and the accumulation of these species on the photocatalysts surface has been considered as the main cause for the deactivation [9,10], the evolution of the peak height of the bands assigned to these products was also followed. Fig. 8 shows the normalized ratio of desorbed cyclohexanone over the total amount of cyclohexanone

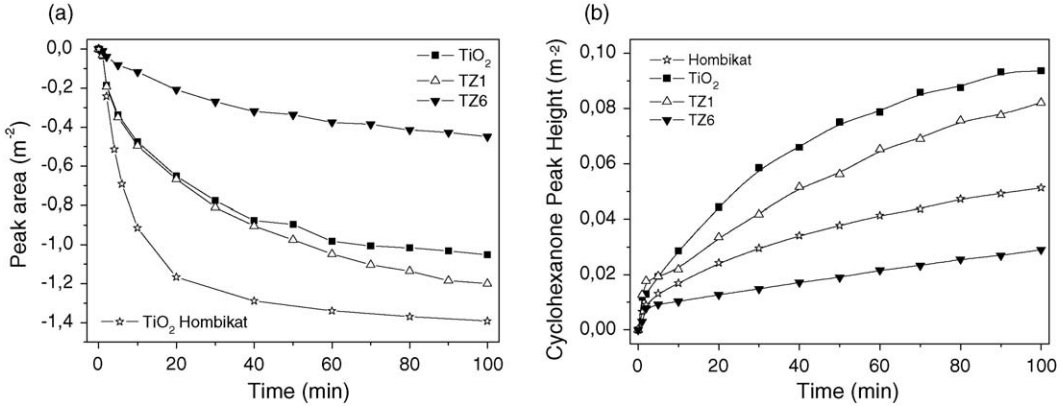


**Fig. 7.** (a) Evolution of cyclohexane during the photo-oxidation reaction on the different catalysts; (b) total cyclohexanone production as a function of illumination time, represented as the sum of the peak height of the bands assigned to cyclohexanone (adsorbed + desorbed). Peak height was normalized by considering the $S_{BET}$ and mass of catalyst employed in the reaction. Commercial $TiO_2$, Hombikat UV100, was used as a reference photocatalyst.

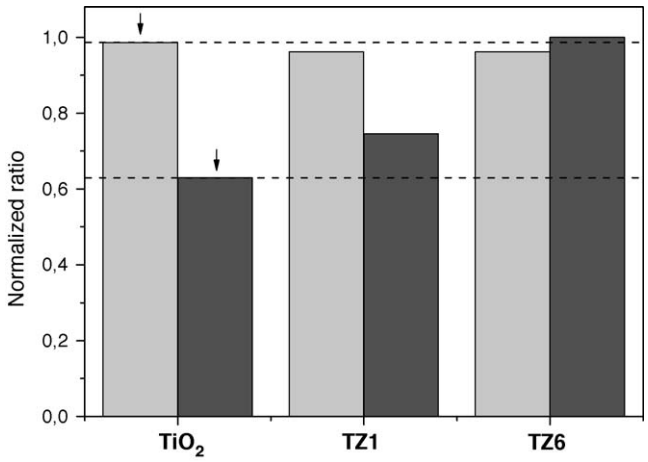


**Fig. 8.** Ratio of desorbed cyclohexanone over the total amount of cyclohexanone detected (light grey bars), and ratio of surface carbonates and carboxylates over adsorbed cyclohexanone (dark grey bars). Dashed lines and arrows point at the best results obtained in this work.

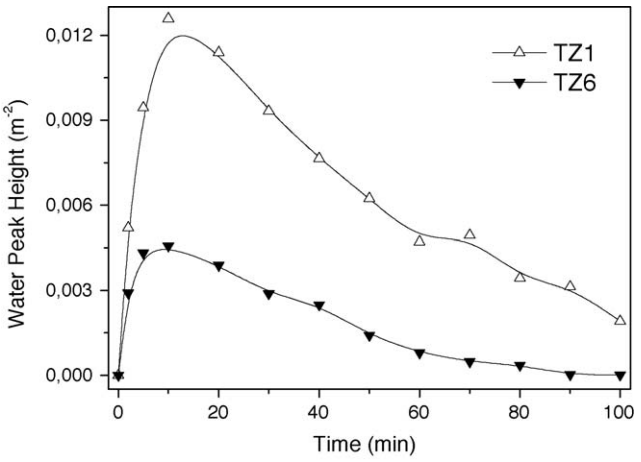


**Fig. 9.** Evolution of water during the photo-oxidation of cyclohexane on TZ1 and TZ6. Peak height (at ca. 3400 $cm^{-1}$) was normalized by considering the $S_{BET}$ and mass of catalyst employed in the reaction.

formed in the reaction, and the normalized ratio of surface carbonates and carboxylates over adsorbed cyclohexanone, respectively. The differences among the tested materials in amount of desorbed cyclohexanone are negligible. Clearly the relative amount of carboxylates and carbonates is increasing upon the addition of Zr to the $TiO_2$ catalyst.

Further information on the effect of Zr on the photo-activity of $TiO_2$ can be derived from the development of the water bands. The time evolution of the adsorbed water, followed by the peak height at ca. 3400 $cm^{-1}$, is displayed in Fig. 9. It can be observed that there is an increase in the peak height in the initial stages of the reaction, followed by a strong decrease in the spectral intensity of the band after 10–20 min of irradiation. TZ6 presents the lowest production of water and also the slowest consumption rate. TZ1 produces considerably more water, comparable to unpromoted $TiO_2$ (not shown).

## 4. Discussion

Although a wide number of references can already be found in the literature related to the selective photo-oxidation of cyclohexane, to the best of our knowledge the relation between the surface characteristics and the performance of $TiO_2$-based photocatalysts has not been studied intensively. As described in the previous section, the incorporation of Zr into the anatase lattice, up to 6 at.% Zr content, does not introduce important modifications in the anatase structure. Zr atoms are randomly substituting Ti in the lattice, leading only to a slight increase in the strain and in the cell volume, the latter due to the bigger size of $Zr^{4+}$ with respect to $Ti^{4+}$. Furthermore, particle size is also being insignificantly modified by the doping. On the other hand, the selected photocatalysts exhibit surface modifications with respect to undoped $TiO_2$, whose magnitude increases with increasing the Zr doping level. It is worth reminding that the ATR-FTIR data were normalized to surface area to eliminate the effect of the observed increase in the $S_{BET}$ of the doped photocatalysts and fairly analyze the intrinsic activity of the surface sites.

Fig. 10 summarizes the correlation observed between the performance of the photocatalysts in the selective oxidation of cyclohexane and the studied surface properties. The key factors that seem to be influencing the behaviour of the materials are, on one hand, the number, strength and distribution of acid sites and, on the other hand, the hydrophilicity of the surface. The hydrophilicity of the samples was estimated from the DRIFT spectra of the catalysts, by considering the water loss percentage with increasing temperature. Both surface acidity and hydrophilicity grow parallel with increasing Zr content, consistent with the observations of Góra-Marek et al. [35].

The photo-oxidation results obtained from the ATR-FTIR measurements point out that cyclohexanone production decreases with increasing Zr content (Fig. 7b) or, in other words, with increasing hydrophilicity and surface acidity. The low activity of the TZ6 sample can be associated with inhibited cyclohexane adsorption on its surface (Fig. 5a), due to the higher hydrophilicity of this material. Water molecules adsorbed on the surface of the catalyst, or formed during the reaction, can limit the adsorption of the non-polar cyclohexane molecules on low-coordinated $Ti^{4+}$ and $O^{2-}$ ions [25,36,37], considered as the adsorption and photocatalytically active sites in anatase [20]. Water molecules strongly bound to the surface could also hamper $O_2$ adsorption, favouring the electron-hole recombination, and decreasing the catalyst activity [37,38].

On the other hand, the amount of carboxylates and carbonates accumulated on the surface increases with Zr incorporation. These products, whose strong adsorption on the catalyst surface has been considered the main reason for catalyst deactivation, are proposed to be mainly formed from further oxidation of adsorbed cyclohexanone molecules [10]. Since no significant differences in the ratio of adsorbed vs. desorbed cyclohexanone could be found, an alternative route for excessive carboxylate formation could be the non-selective decomposition of the cyclohexyl peroxide intermediate. This secondary route might be favoured by the larger hydrophilicity of this sample, and the related higher concentration of water born $OH^{\bullet}$ radicals, leading to non-selective products. Data shown in Fig. 7a and b confirm this statement, showing that a higher cyclohexane oxidation rate on TZ1 does not lead to a higher cyclohexanone production, the result of a higher amount of non-selective products formed (carboxylates and carbonates). A similar behaviour is observed for commercial $TiO_2$, Hombikat UV100.

The presence of at least two different types of sites on the catalyst surface can be considered [39,40]. The first type would be related to the five-fold coordinated Ti atoms. These centers, acting as Lewis acid sites due to their low coordination, are considered as strong adsorption sites, suitable for both cyclohexane and water adsorption. The second type, more hydrophilic, would be associated with the surface hydroxyls and bridging oxygens and, because of their more polar character, would be less suitable for

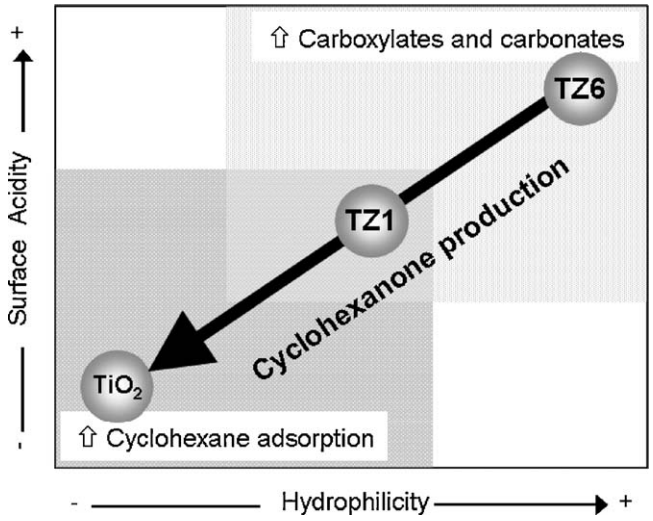


**Fig. 10.** Schematic representation of the qualitative relationship between the surface properties and the observed performance of the catalysts in the selective photo-oxidation of cyclohexane.

cyclohexane adsorption and more appropriate for water molecules and partially oxidized compounds. Furthermore, these hydroxyl groups could be involved in the non-selective secondary route. Further analysis is needed to elucidate the role of the various surface OH-groups and $O_2$ in the selective photo-oxidation of liquid cyclohexane, as well as the contribution of surface water to the product distribution. This will lead to guidelines for further catalyst optimization.

## 5. Conclusions

A reverse microemulsion method has allowed us to obtain materials with the same structure and electronic properties, but different surface characteristics. The photocatalytic oxidation of cyclohexane was performed over undoped $TiO_2$ and $Ti_{1-x}Zr_xO_2$ ($x = 0.01$ and 0.06), and analyzed *in situ* by means of ATR-FTIR spectroscopy. Despite the frequently reported beneficial effect of increasing acidity in different catalytic reactions [20,41–45], and an expected promotion of the selective decomposition of the cyclohexyl peroxide intermediate to the desired product, an increase in the Brønsted acidity, together with a higher hydrophilicity, have been proven to decrease the surface selectivity and stability of the catalyst. This is mainly the result of an enhanced number of water born $OH^{\bullet}$ radicals, inducing non-selective reactions, and enhanced hydrophilicity leading to slow desorption and consecutive oxidation of cyclohexanone.

## Acknowledgements

MDHA wants to thank the *Spanish Science and Technology Foundation* (FECYT) and *Ministerio de Ciencia e Innovación* for the award of her postdoctoral contract. ARA and GM gratefully acknowledge NWO/STW in the framework of the VIDI program for financial support. The authors want to thank also the "*Centro de Microscopía Luis Bru*" for the TEM images and Dr. B. Bachiller-Baeza for the microcalorimetric measurements.

## References

[1] W.B. Fisher, J.F. Van Pepper, M. Grayson (Eds.), 3rd ed., Kirk-Othner Encyclopedia of Chemical Technology, vol. 7, Wiley, New York, 1979, p. 411.
[2] W. Mu, J.M. Herrmann, P. Pichat, Catal. Lett. 3 (1989) 73.
[3] G. Lu, H. Gao, J. Suo, S. Li, J. Chem. Soc., Chem. Commun. (1994) 2423.
[4] A. Sclafani, J.M. Herrmann, J. Phys. Chem. 100 (1996) 13655.
[5] P. Boarini, V. Carassiti, A. Maldotti, R. Amadelli, Langmuir 14 (1998) 2080.
[6] C.B. Almquist, P. Biswas, Appl. Catal. A: Gen. 214 (2001) 259.
[7] X. Li, G. Chen, Y. Po-Lock, C. Kutal, J. Chem. Technol. Biotechnol. 78 (2003) 1246.
[8] M.A. Brusa, M.A. Grela, J. Phys. Chem. B 109 (2005 1914).
[9] P. Du, J.A. Moulijn, G. Mul, J. Catal. 238 (2006) 342.
[10] A.R. Almeida, J.A. Moulijn, G. Mul, J. Phys. Chem. C 112 (2008) 1552.
[11] M.D. Hernández-Alonso, J.M. Coronado, B. Bachiller-Baeza, M. Fernández-García, J. Soria, Chem. Mater. 19 (2007) 4283.
[12] G. Mul, G.M. Hamminga, J.A. Moulijn, Vib. Spectrosc. 34 (2004) 109.
[13] A. Fuerte, M.D. Hernández-Alonso, A.J. Maira, A. Martínez-Arias, M. Fernández-García, J.C. Conesa, J. Soria, G. Munuera, J. Catal. 212 (2002) 1.
[14] T. Ungár, A. Borbély, Appl. Phys. Lett. 69 (1996) 3173.
[15] G.K. Williamson, W.H. Hall, Acta Metall. 1 (1953) 22.
[16] H. Savaloni, M. Gholipour-Shahraki, M.A. Player, J. Phys. D: Appl. Phys. 39 (2006) 2231.
[17] T. Ungár, A. Borbély, G.R. Goren-Muginstein, S. Berger, A.R. Rosen, Nanostruct. Mater. 11 (1999) 103.
[18] A. Auroux, Top. Catal. 4 (1997) 71.
[19] B. Dragoi, A. Gervasini, E. Dumitriu, A. Auroux, Thermochim. Acta 420 (2004) 127.
[20] X. Fu, L.A. Clark, Q. Yang, M.A. Anderson, Environ. Sci. Technol. 30 (1996) 647.
[21] Y.R. Do, W. Lee, K. Dwight, A. Wold, J. Solid State Chem. 108 (1994) 198.
[22] J. Papp, S. Soled, K. Dwight, A. Wold, Chem. Mater. 6 (1994) 496.
[23] K. Tanabe, T. Sumiyoshi, K. Shibata, T. Kiyoura, J. Kitagawa, Bull. Chem. Soc. Jpn. 47 (1974 1064).
[24] C.L. Thomas, Ind. Eng. Chem. 41 (1949) 2564.
[25] J. Soria, J. Sanz, I. Sobrados, J.M. Coronado, A.J. Maira, M.D. Hernández-Alonso, F. Fresno, J. Phys. Chem. C 111 (2007) 10590.
[26] P.A. Connor, K.D. Dobson, A.J. McQuillan, Langmuir 15 (1999) 2402.
[27] K.S. Finnie, D.J. Cassidy, J.R. Bartlett, J.L. Woolfrey, Langmuir 17 (2001) 816.
[28] M. Scheithauer, T.-K. Cheung, R.E. Jentoft, R.K. Graselli, B.C. Gates, H. Knözinger, J. Catal. 180 (1998) 1.
[29] T. Shimanouchi, Tables of Molecular Vibrational Frequencies Consolidated Volume I, vol. I, National Bureau of Standards, Washington, DC, 1972.
[30] L.J. Bellamy, The Infrared Spectra of Complex Molecules: Advances in Infrared Group Frequencies, 3rd ed., Chapman nd Hall Ltd., London, 1975.
[31] D.J. Yates, J. Phys. Chem. 65 (1961) 746.
[32] A.A. Davydov, Infrared Spectroscopy of Adsorbed Species on the Surface of Transition Metal Oxides, John Wiley & Sons, West Sussex, 1990.
[33] D. Bianchi, T. Chafik, M. Khalfallah, S.J. Teichner, Appl. Catal. A: Gen. 105 (1993) 223.
[34] J.C. Lavalley, Catal. Today 27 (1996) 377.
[35] K. Góra-Marek, J. Datka, Appl. Catal. A: Gen. 302 (2006) 104.
[36] L.A. Phillips, G.B. Raupp, J. Mol. Catal. 77 (1992) 297.
[37] L. Cao, Z. Gao, S.L. Suib, T.N. Obee, S.O. Hay, J.D. Freihaut, J. Catal. 196 (2000) 253.
[38] D.R. Park, J. Zhang, K. Ikeur, H. Yamashita, M. Anpo, J. Catal. 185 (1999) 114.
[39] M. Lewandowski, D.F. Ollis, Appl. Catal. B: Environ. 43 (2003) 309.
[40] M. Lewandowski, D.F. Ollis, Appl. Catal. B: Environ. 45 (2003) 223.
[41] D. Kozlov, D. Bavykin, E. Savinov, Catal. Lett. 86 (2003) 169.
[42] K.K. Akurati, A. Vital, J.-P. Dellemann, K. Michalow, T. Graule, D. Ferri, A. Baiker, Appl. Catal. B: Environ. 79 (2008) 53.
[43] T. Onfroy, G. Clet, M. Houalla, J. Phys. Chem. B 109 (2005) 14588.
[44] X. Wang, J.C. Yu, P. Liu, X. Wang, W. Su, X. Fu, J. Photochem. Photobiol. A 179 (2006) 339.
[45] H. Zou, Y.S. Lin, Appl. Catal. A: Gen. 265 (2004) 35.